Role of Low Temperature Resistivity on Fast Electron Transport in Disordered Aluminium and Copper

David R Blackman,[1] A.P.L.Robinson,[2] and John Pasley[1]
[1)] *York Plasma Institute*
Department of Physics, University of York
Heslington, York, YO10 5DD UK
[2)] *Central Laser Facility*
STFC Rutherford Appleton Laboratory
Harwell Oxford, Didcot, Oxfordshire, OX11 0QX UK

(Dated: 12 May 2015)

To determine the link between the onset of the filamentation instability and the low temperature resistivity of the cold-electron plasma a comparison between the transport of fast electrons through disordered aluminium and copper targets is made using the hybrid code Zephyros. The filamentation instability is suppressed at laser intensities below $5\times10^{19}Wcm^{-2}$ for materials where the resistivity of the material is lower than $1\mu\Omega m$ at 1eV. Interestingly copper targets show larger resistive magnetic field growth, and as a result more collimation of the electron beam, despite having a consistently smaller resistivity at lower temperatures than that of aluminium. The increase in magnetic field strength is responsible for the suppression of the filamentation instability. This is due to the resistive filamentation growth rate for copper and aluminium, under identical conditions, being numerically very close.

I. INTRODUCTION

The propagation of relativistic electron beams in laser-solid interactions is a central topic in several applications of ultra-intense lasers, including the fast ignition[1,2] approach to fusion and proton[3–5] or ion[6] acceleration applications. The spread of the electron beam is of particular importance in fast ignition due to the desire to deposit near all of the fast electron energy in a locality of similar size to the source over a stand-off distance many times these transverse sizes[2].

The filamentation of laser-driven fast electron currents in solid targets has been observed in several previous experiments[7,8]. There have also been several studies into the formation of filaments via the beam-Weibel instability[9,10] caused by differing conditions in the target including both density modulations and target resistivity[11]. The motion of the cold-electron background and resistively generated magnetic fields have been shown to have a critical impact on the behaviour of fast electron beams[12,13]. Bell and Kingham[14] demonstrated the link between the growth of magnetic fields and the self collimation of electron beams through solid materials using a simple rigid beam model. The effect of changing the crystal structure of the target materials has also been studied[8,15]. Crystalline allotropes of carbon were found to suppress filament growth whilst isotropic disordered allotropes did not. The role of resistively generated magnetic fields in collimating an electron beam has also been investigated using a proton beam to selectively heat parts of a target to induce lattice melting[16]. In order to suppress the formation of filaments the electron beam can be confined to tightly collimated beams. This collimating effect has been observed in nano-structured targets made from carbon nano-tubes[17], nano-channels fabricated from metallic elements[18] where the transverse motion of the fast electrons was limited by the channels.

In order to understand the effect of low temperature resistivity on fast electron transport we have studied the disordered forms of two materials with significantly different Z: aluminium and copper. The disordered state can occur either due to the materials being an amorphous alloy, or due to melting from the solid state. The hybrid code Zephyros was used to study the transport of electrons through these materials driven by a range of laser intensities. The resistivity of the background electron fluid is modelled using the Lee-More resistivity model[19], and the Thomas-Fermi model was used to determine the ionisation state. Two important results are obtained from this study: Firstly that materials with a lower peak resistivity tend to exhibit larger collimating magnetic fields which act to suppress filament formation, and, secondly, that this magnetic field growth is due to a lower rate of heating in those materials. The role of the cold electron resistivity in suppression of the filamentation instability is examined analytically and shows little change across the two materials again indicating that the magnetic field growth is the main mechanism for suppression of filaments in this case.

II. SIMULATION METHODOLOGY

Zephyros is a hybrid fast-electron code which uses a particle-in-cell model for the fast electron modelling with a static fluid to represent the background electrons. The simulated targets have dimensions $200\times200\times50\mu m^3$, consisting of cubic cells $0.5\mu m$ to a side, with the laser normal to the largest surface. An assumption of a disordered ion spatial distribution is used, which implies an isotropic cold-electron mean-free path (m.f.p.). To simulate the effect of the laser-plasma interaction fast

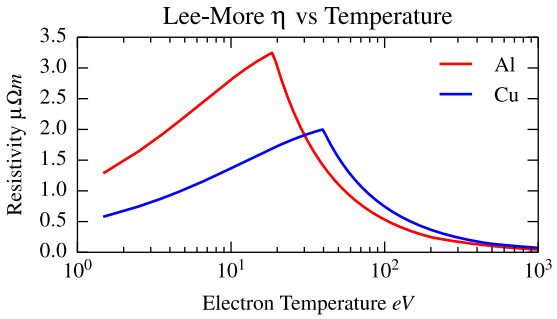

FIG. 1. Reduced Lee-More resistivity curves for Aluminium and Copper with an effective cold-electron m.f.p. equal to the inter-atomic spacing at the solid density of the two metals.

electrons were injected into the target across a focal spot with a FWHM of $9.4\mu m$ and with a uniform injection angular distribution up to a maximum of 70° half angle. There were a total of 5×10^7 macro-particles used in each simulation which were gradually injected over the total length of the pulse, $t_l = 800fs$, at each time-step according to a top-hat distribution. The pulse length is chosen simply so that there is sufficient time for the fast electrons to propagate to the far side of the target during the laser pulse. The electrons have an energy spectrum determined using the ponderomotive scaling where $T_f = m_e c^2(\left(0.73 I_{18}\lambda^2_{\mu m} + 1\right)^{1/2} - 1)$ and $I_{18} = 1 \times 10^{18} W cm^{-2}$. To calculate the scaling an effective laser wavelength $\lambda = 1.053\mu m$ is chosen to be consistent with an Nd:glass laser system. The intensity is varied from 0.1 to 5 $\times 10^{20} W cm^{-2}$ which given the scaling described produces an electron distribution with T_f varying between 1 and $10MeV$. The initial temperature of the targets were set to 1eV, which assumes a high-contrast laser-pulse.

An implementation of the Lee-More[19] resistivity model was chosen as certain experiments[20] have compared well to theoretical predictions using this model, which along with it being relatively easy to implement, has lead to its widespread use. The two materials, disordered allotropes of aluminium and copper, were chosen so that their atomic number and solid density were different enough that the Lee-More model would give significantly different resistivity profiles. In this implementation, rather than use the prescription given in the original Lee-More model for the minimum m.f.p., we specify the minimum cold-electron m.f.p. as an input parameter to the model. We chose the initial cold-electron m.f.p. to be set isotropically to the inter-atomic spacing (r_s) (1.62Å for Al and 1.45Å for Cu) to simulate disordered ion spatial distributions. The two resistivity profiles can been seen in fig.1. The resistivity profile calculated for copper peaks at a higher temperature but lower resistivity when compared to the aluminium profile ($2\mu\Omega m$ at 40eV for Cu vs. $3.2\mu\Omega m$ at 19eV for Al).

III. COMPARISON OF COPPER AND ALUMINIUM TRANSPORT

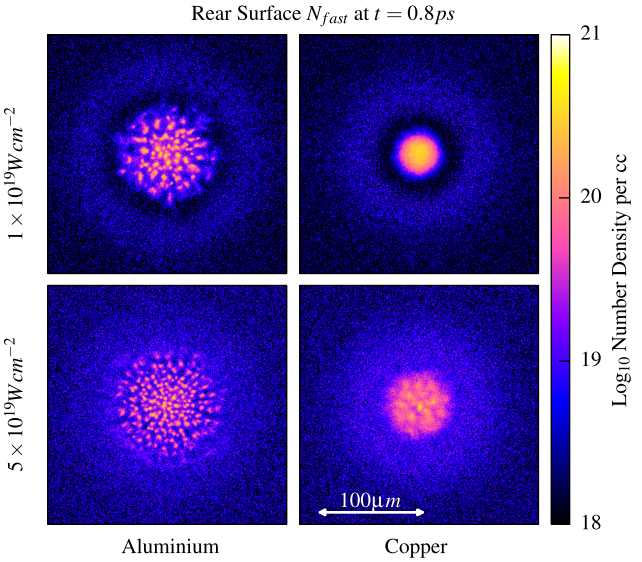

FIG. 2. Rear surface fast electron density plots of aluminium (left) and copper (right). At the lowest intensity (top row $10^{19} W cm^{-2}$) copper shows no filamentation at all whilst aluminium shows a significant amount. At a slightly increased intensity of $5 \times 10^{19} W cm^{-2}$ (bottom row) there are a small number of more diffuse filaments in the copper, whilst the aluminium retains a large number of tight filaments. The halo-like features observable in the top two plots are refluxing electron populations.

The fast electron transport pattern in each simulation can be examined by looking at transverse and longitudinal slices of the fast electron density at later times. Fig.2 shows rear surface plots of the fast electron density at the end of the laser pulse (t=800fs), from these it is immediately obvious that there is a significant difference in the propagation of the electron beams through the two materials. The copper target at the lowest intensity showed a highly collimated beam terminating in a tight dense spot whilst the aluminium target shows multiple smaller spots indicating a highly filamented beam. When the laser intensity is raised to $5 \times 10^{19} W cm^{-2}$, the copper then shows a slight breaking up of the beam. In order to summarise results from all of these simulation runs; several line-outs were taken out of the centre of the n_{fast} profiles in fig.2 and a Fourier spectrum of each was taken (see fig.3). To avoid being limited by noise these spectra were then averaged.

The spectra in fig.3 show the relative prominence of features at particular scale lengths. A spectra showing a lot of features around the 5-15 micron level would denote a fragmented rear spectrum indicating filamentation of the electron beam. Conversely a spectra showing

a dominance of features around the 50-100 micron level would indicate a collimated beam. Only the lowest intensity copper target simulation shows collimation of the electron beam with negligible filamentation.

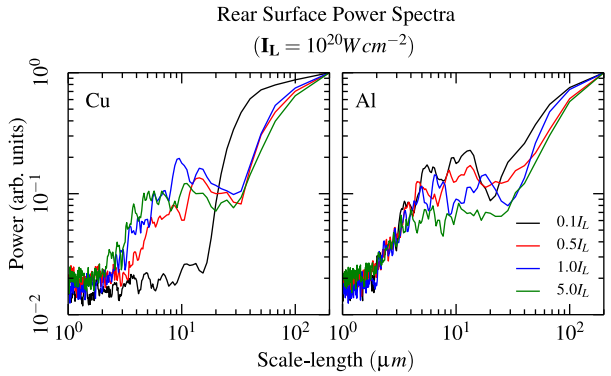

FIG. 3. Power spectra of rear surface fast electron density features for aluminium (left) and copper (right). These spectra show how often features occur at particular scale lengths, in simulations where fast electron filamentation has occurred there is a significant rise in the quantity of features around the 5-10 micron size. It clear from these plots that the filamentation instability is turned off for copper at low intensities.

IV. MAGNETIC FIELD AND RESISTIVITY

There is a remarkable difference in the global B-field in copper versus aluminium, namely that it has a larger magnitude and is has a more cylindrical shape in copper. This is curious given the lower peak resistivity of Cu. Here we show we can explain this through a simple rigid beam model[21]. The magnetic field along the axis of propagation is shown for both targets in fig.5. Earlier growth of the magnetic field in the aluminium case appears to promote the growth of filamentary structures. At around 10 microns away from the injection region linear modulations appear in the magnetic field in the aluminium target, whilst the copper target shows strong magnetic fields acting to confine the beam at this point.

The higher low temperature resistivity in the aluminium target allows fine structures to grow more quickly in the magnetic field. These fine scale structures act to promote the divergent filamentation of the electron beam, with narrow B-field channels forming acting to individually collimate beam filaments leading to a refinement of the fine scale structure. Conversely in the copper target, where the low temperature resistivity is smaller, larger scale magnetic fields tend to grow which can then act to collimate the beam and suppress smaller scale magnetic field growth. Whilst the fine scale structures are still evident in the copper target, the large scale collimating fields confine the electrons to a narrow channel suppressing the smaller scale filament growth.

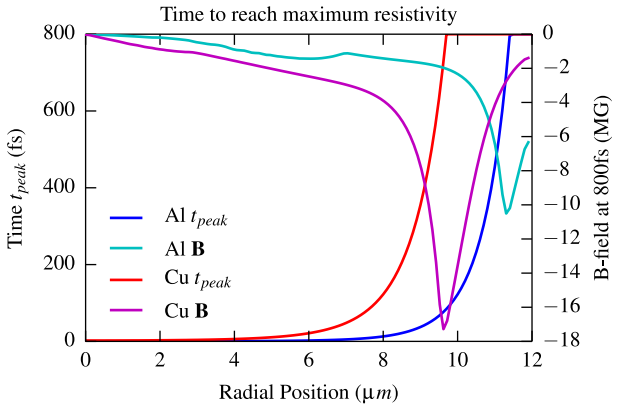

FIG. 4. Time taken to reach the peak resistivity as a function of distance from the the center of the beam in the two materials, this was calculated using the rigid beam model. The increase in t_{peak} with distance matches up well with final B-file profile calculated using the rigid beam model.

In order to explain the larger magnetic fields seen in

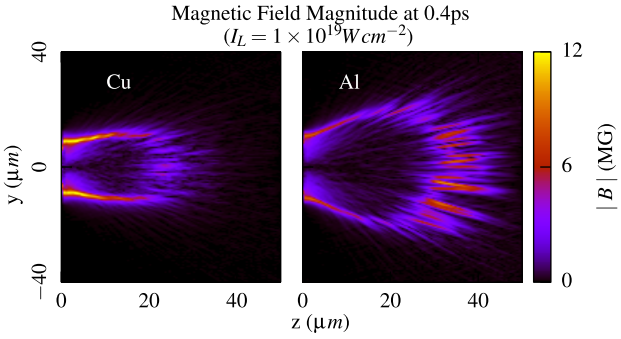

FIG. 5. Plots of the magnetic fields after 0.4ps of growth, halfway into the 0.8ps laser pulse. The aluminium target shows magnetic field growth almost all the way across the target to the rear side where as the copper target has a much more compact magnetic field structure locate towards the source of the fast electrons.

the copper target a rigid beam calculation[21], considering only Ohmic heating (eqn.1) and resistive magnetic field growth (eqn.2) is used to calculate the expected magnetic fields. The fast electron current J_f is considered as a rigid beam of electrons with a Gaussian profile decreasing with r. To keep the analysis consistent, the Lee-More model was used for the resistivity, and a simple fit from the Thomas-Fermi model for n_e was employed.

$$\frac{dT}{dt} = \frac{J_f^2 \eta(T)}{\frac{3}{2} n_e(T) e} \tag{1}$$

$$\frac{dB}{dt} = -\nabla(\eta(T) J_f(r)) \tag{2}$$

Fig.6 shows much larger magnetic field growth closer

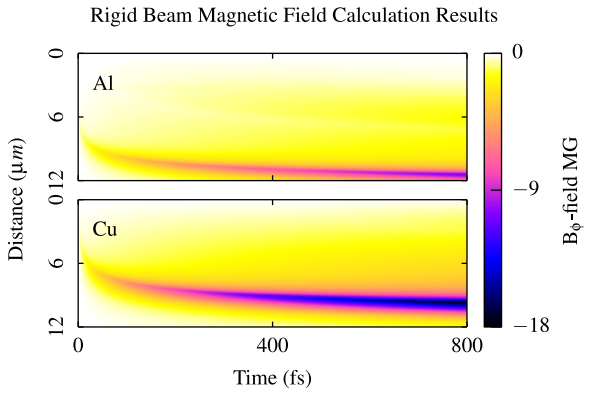

FIG. 6. Magnetic field calculations made using a rigid-beam model, the copper target shows a significantly larger magnetic field compared to the aluminium target. The distance from the centre of the beam to the peak magnetic field is much smaller in the copper target than the aluminium.

to the centre of the beam in the copper target as compared to the aluminium target. The main reason for the larger fields in the copper target is the consistently lower resistivity at low temperatures. This allows for a lower rate of heating whilst still providing enough resistivity to generate significant magnetic fields for a longer length of time before slipping into the Spitzer regime where the growth of the magnetic fields is significantly lower. The time taken to reach the peak resistivity is also of interest as this time is the point at which the Lee-More model switches to using the Spitzer treatment significantly lowering the resistivity in the material, this can be seen in fig.4. The B-field calculated by the rigid beam model and t_{peak} peak at the same point in both the copper and aluminium calculations as can also be seen in fig.4. An approximate time taken to reach peak resistivity, and so the peak growth of the magnetic fields, can be found using a simpler treatment that given by the Lee-More model. Given a simplistic approximation where $\tau = \frac{\mathrm{d}_{ion}}{v_t h}$ and d_{ion} is the inter-atomic spacing of the material, and substituting for v_{th}, we can now write:

$$\eta = \frac{m_e}{e^2 n_e \tau} = \frac{m_e}{e^2 n_e \mathrm{d}_{ion}} \sqrt{\frac{k_B T_e}{m_e}} \tag{3}$$

The electron density predicted by the TF model varies considerably with temperature in the region between 1 and 40eV. However, given $n_e = n_i Z(\frac{Z_{eff}}{Z})$, the relative ionisation (Z_{eff}/Z) of both materials have very similar temperature profiles. If the ratio of the peak times is calculated the variation in the relative ionisation in the two materials cancels out. Equation 1 can then be integrated between 1 and 40eV to give the time taken to reach the peak temperature, the ratios of these two times can be equated as follows:

$$\frac{t_{Al}}{t_{Cu}} = \frac{n_{iAl}^2 Z_{Al}^2}{n_{iCu}^2 Z_{Cu}^2} \sim 0.1 \tag{4}$$

This result also matches up with the numerical treatment used in the rigid beam model where at the center of the beam at peak J_{fast} copper $t_{peak} = 2.24fs$ and aluminium $t_{peak} = 0.236fs$. Taking the peak resistivity from the Lee-More model used previously, the magnetic field can be given the same treatment as the time to reach peak η to give:

$$\frac{B_{Al}}{B_{Cu}} = \frac{\eta_{Alpeak} t_{Al}}{\eta_{Cupeak} t_{Cu}} \sim 0.16 \tag{5}$$

This treatment, though admittedly simplistic, does show a magnetic field strength that has a strong dependence on the time spent at low temperatures, i.e. time spent outside of the Spitzer regime.

V. RESISTIVITY DEPENDANT EFFECTS

The Lee-More[19] model can be used with an arbitrary choice of the minimum m.f.p. for the electrons. So far in this paper we have taken this to be the interatomic spacing, and this is also the absolute minimum for the m.f.p. in the original Lee-More model. However we should note that in the original Lee-More, when the electron m.f.p. did not fall below the interatomic spacing, the minimum m.f.p. was determined using the Bloch-Grüneisen formula complemented by an expression to account for melting. Since we assume that our target is already highly disordered/molten already, our approach actually ends up being equivalent to the orignal Lee-More approach for the case where the target temperature is well above the melting temperature. The value of the absolute limit on the minimum electron m.f.p. is, however, open to question, and varying this value can have a substantial effect on the resistivity curve. To study the effect of changing this parameter on the magnetic field growth in absence of any other factor an altered version of the Lee-More model was calculated where the low temperature cold-electron m.f.p. was multiplied by a factor which was chosen to be 2, 4 or 8. The newly altered resistivity profiles are shown in fig.7.

By altering the resistivity profile of the aluminium at low intensities it is possible to suppress the filamentation of the electron beam enough to get significant collimation and confine the beam to $\sim 20\mu m$. Fig.8 show the newly generated feature spectra for aluminium targets with the altered resistivity profiles. In the targets where the resistivity approaches more than $0.5\mu\Omega m$ at a temperature of 1eV or below filamentation occurs and shows a multitude of tightly confined filaments. Above this limit and the electron beams are collimated. There is, however, a borderline case $l_{mfp} = 4r_s$, which shows less well defined individual filaments that are held together in a large scale collimating magnetic field. These collimating fields are a result of low resistivity at low temperatures, meaning less ohmic heating at earlier times and larger magnetic fields as a result. Whether the filaments are suppressed

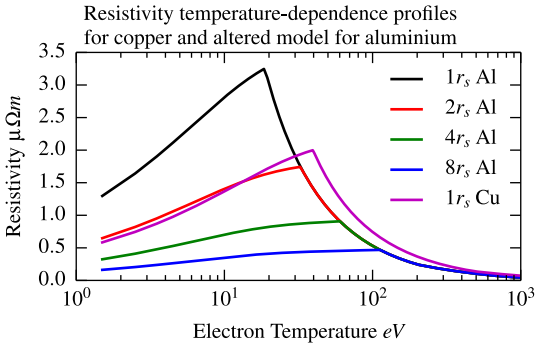

FIG. 7. Plot comparing the resistivity of aluminium with different assumed cold-electron m.f.p. lengths alongside copper at the shortest assumed m.f.p. length.This comparison shows a similarity in the cold resistivity between the longest aluminium m.f.p. and the shortest copper m.f.p..

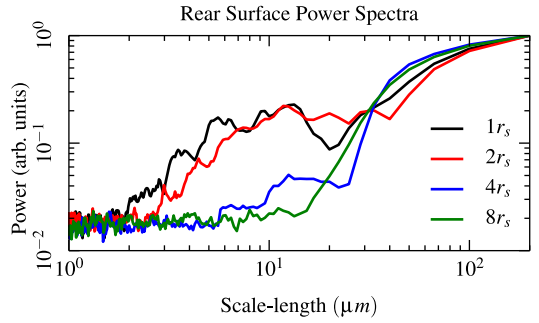

FIG. 8. This plot show the effect of increasing the m.f.p. of the cold-electron background, which effectively lowers the resistivity calculated by the Lee-More algorithm. Increasing the m.f.p. beyond twice the inter-atomic spacing results in a smooth profile with no filamentation.

by the large collimating fields or that they do not grow as a result of lower resistivity is a question that needs to be answered. Starting with Faraday's law, Ohm's law and a linearised set of fluid equations the growth rate for the resistive filamentation instability can be found[11] (which is also quite similar to an earlier treatment by Molvig[22]) so that this time-scale can be compared to the growth of the larger scale magnetic fields. Given Faraday's law:

$$\frac{\partial \mathbf{B}}{\partial t} = -\nabla \times \mathbf{E} \tag{6}$$

and Ohm's law:

$$\mathbf{E} = -\eta \mathbf{j}_f \tag{7}$$

and considering a two dimensional geometry with an isotropic resistivity and $j_x = J_{fast}$ we can write:

$$\frac{\partial B_z}{\partial t} = \eta \frac{\partial j_x}{\partial y} \tag{8}$$

The system is then perturbed so that $n_f = n_{f0} + n_1$, $u_{fy} = u_{y1}$, $u_{fx} = u_{x0}$ and $\gamma = \gamma_0$. Using these perturbations and only considering first order terms gives a linearised continuity equation:

$$\frac{\partial n_1}{\partial t} + n_{f_0} \frac{\partial u_{y_1}}{\partial y} = 0 \tag{9}$$

The magnetic portion of the Lorentz force (linearised again) can be written for the fast electrons as:

$$\frac{\partial u_{y_1}}{\partial t} = \frac{e u_{x_0} B_z}{\gamma_0 m_e} \tag{10}$$

Taking the density (and therefore current) perturbations to be sinusoidal, the velocity (and therefore magnetic field) must be 90° out of phase, giving $n_1 = n_{f_0}\mathrm{N(t)}\cos(ky)$, $J_{fast} = J_{fast}\mathrm{N(t)}\cos(ky)$, $u_{y_1} = u\sin(ky)$, and $B_z = B\sin(ky)$. Substituting into the continuity9, Lorentz 10 and the modified Faraday/Ohm's law equation 8 and cancelling out the sinusoidal functions gives:

$$\frac{\partial B}{\partial t} = -\eta J_{fast}\mathrm{N}k \tag{11}$$

$$\frac{\partial \mathrm{N}}{\partial t} = -ku \tag{12}$$

and

$$\frac{\partial u}{\partial t} = \frac{e u_{x_0}}{\gamma m_e} B \tag{13}$$

Repeatedly differentiating and substituting for N in equations 11,12 and 13 gives:

$$\frac{\partial^3 \mathrm{N}}{\partial t^3} = \frac{\eta k^2 e u_{x_0} J_{fast}}{\gamma_0 m_e}\mathrm{N} \tag{14}$$

This differential equation has a solution of the form:

$$N \propto e^{gt} \tag{15}$$

Where

$$g = \left[\frac{\eta k^2 e u_{x_0} J_{fast}}{\gamma_0 m_e}\right]^{1/3} \tag{16}$$

Given that the growth factor, $g \propto \eta^{1/3}$, a change (at 1eV) from $\eta_{Al} = 1.07\mu\Omega m$ to $\eta_{Cu} = 0.48\mu\Omega m$ yields a growth rate in copper of 76% of that in aluminium. At the lowest laser intensity the filaments in the copper target are completely suppressed and a strongly collimated beam is observed. This behaviour is likely not due to the reduction in the filamentation growth rate, which is in itself due to the change in resistivity across the two materials, but lies with the larger magnitude and scale magnetic fields observed in the copper target.

VI. CONCLUSIONS

The filamentation of the electron beam in a high-intensity laser-plasma interaction is critically dependant on the magnitude and typical feature size in the resistive magnetic fields generated by drawing of a cold-electron return current. In this simulation-based study several hybrid fast electron simulations were used to investigate disordered forms of aluminium and copper. The following observations were drawn from the results of these simulations: The simulations where the low-temperature resistivity is high were seen to have significantly higher levels of filamentation, indicating a critical relationship between the starting resistivity and the onset of filamentary structures in the electron beam. The resulting magnitude and scale-length of the later magnetic fields, in the material with the higher resistivity, was significantly smaller than that of the lower resistivity material. The heating effect attributed to high resistivity materials has a very important effect on the growth of the magnetic fields within them, with higher resistivity effectively stunting the growth of large collimating magnetic fields allowing small transverse scale filamentation to occur. Conversely a lower rate of heating allows for significantly larger fields to grow resulting in far more effectively collimated electron beams and suppression of filamentation. The growth rate of the resistive filamentation instability is not significantly different between the case where there is filamentation to where there is not. This implies that the fact that copper has a lower resistivity is not the sole, or main, cause of the absence of filaments where the beam is collimated. This collimation is, however, due to the fact that high resistivity materials are heated more quickly and so the enter the Spitzer resistivity regime much sooner, where the resistivity drops to a much lower level than when cold. These conclusions are supported by a simple analysis of the case of a rigid beam of fast electrons traversing a resistive medium and a simple analytic model of the filamentation growth rate.

VII. ACKNOWLEDGEMENTS

JP would like to acknowledge the Engineering and Physical Science Research Council's grant EP/I030018/1, AR would also like to acknowledge the European Research Council's STRUCMAGFAST grant ERC-StG-2012 and DB would like to acknowledge the Engineering and Physical Science Research Council's grant EP/K504178/1. The authors are grateful for the use of computing resources provided by Science and Technology Facilities Council's e-Science facility.

[1] J. J. Honrubia and J. Meyer-ter Vehn, Plasma Physics and Controlled Fusion **51**, 15 (2008), arXiv:0811.1760.
[2] A. P. L. Robinson, D. J. Strozzi, J. R. Davies, L. Gremillet, J. J. Honrubia, T. Johzaki, R. J. Kingham, M. Sherlock, and A. A. Solodov, Nuclear Fusion **54**, 054003 (2014).
[3] F. Amiranoff, Measurement Science & Technology **12**, 1795 (2001).
[4] J. Davies, Laser And Particle Beams **20**, 243 (2002), conference on Matter in Super-Intense Laser Fields: Short Pulse Super-strong Laser-Plasma Interactions, S Feliu De Guixols, Spain, Sep 29-Oct 04, 2001.
[5] D. A. Maclellan, D. C. Carroll, R. J. Gray, N. Booth, B. Gonzalez-Izquierdo, H. W. Powell, G. G. Scott, D. Neely, and P. Mckenna, Laser And Particle Beams **31**, 475 (2013).
[6] H. B. Zhuo, X. H. Yang, C. T. Zhou, Y. Y. Ma, X. H. Li, and M. Y. Yu, Physics of Plasmas **20**, 093103 (2013).
[7] M. Tatarakis, F. N. Beg, E. L. Clark, A. E. Dangor, R. D. Edwards, R. G. Evans, T. J. Goldsack, K. W. D. Ledingham, P. A. Norreys, M. A. Sinclair, M. S. Wei, M. Zepf, and K. Krushelnick, Physical Review Letters **90**, 175001 (2003).
[8] P. McKenna, A. P. L. Robinson, D. Neely, M. P. Desjarlais, D. C. Carroll, M. N. Quinn, X. H. Yuan, C. M. Brenner, M. Burza, M. Coury, P. Gallegos, R. J. Gray, K. L. Lancaster, Y. T. Li, X. X. Lin, O. Tresca, and C. G. Wahlström, Physical Review Letters **106**, 185004 (2011).
[9] L. Gremillet, G. Bonnaud, and F. Amiranoff, Physics of Plasmas **9**, 941 (2002).
[10] J. M. Hill, M. H. Key, S. P. Hatchett, and R. R. Freeman, Physics of Plasmas **12**, 1 (2005).
[11] A. P. L. Robinson, R. J. Kingham, C. P. Ridgers, and M. Sherlock, Plasma Physics and Controlled Fusion **50**, 065019 (2008).
[12] M. E. Glinsky, Physics of Plasmas **2**, 2796 (1995).
[13] M. Storm, A. A. Solodov, J. F. Myatt, D. D. Meyerhofer, C. Stoeckl, C. Mileham, R. Betti, P. M. Nilson, T. C. Sangster, W. Theobald, and C. Guo, Physical Review Letters **102**, 1 (2009).
[14] A. Bell and R. Kingham, Physical Review Letters **91**, 035003 (2003).
[15] D. A. Maclellan, D. C. Carroll, R. J. Gray, N. Booth, M. Burza, M. P. Desjarlais, F. Du, B. Gonzalez-Izquierdo, D. Neely, H. W. Powell, A. P. L. Robinson, D. R. Rusby, G. G. Scott, X. H. Yuan, C. G. Wahlström, and P. McKenna, Physical Review Letters **111** (2013), 10.1103/PhysRevLett.111.095001.
[16] D. A. MacLellan, D. C. Carroll, R. J. Gray, N. Booth, M. Burza, M. P. Desjarlais, F. Du, D. Neely, H. W. Powell, A. P. L. Robinson, G. G. Scott, X. H. Yuan, C.-G. Wahlström, and P. McKenna, Physical Review Letters **113**, 185001 (2014).
[17] G. Chatterjee, P. K. Singh, S. Ahmed, A. P. L. Robinson, A. D. Lad, S. Mondal, V. Narayanan, I. Srivastava, N. Koratkar, J. Pasley, A. K. Sood, and G. R. Kumar, Physical Review Letters **108**, 235005 (2012).
[18] P. K. Singh, I. Chakraborty, G. Chatterjee, A. Adak, A. D. Lad, P. Brijesh, P. Ayyub, and G. R. Kumar, Physical Review Special Topics - Accelerators and Beams **16**, 1 (2013).
[19] Y. T. Lee and R. M. More, Phys. Fluids **27**, 1273 (1984).
[20] J. F. Benage, Physics of Plasmas **7**, 2040 (2000).
[21] J. R. Davies, J. S. Green, and P. A. Norreys, Plasma Physics and Controlled Fusion **48**, 1181 (2006).
[22] K. Molvig, Physical Review Letters **35**, 1504 (1975).